

# Center vortex model for $Sp(2)$ Yang-Mills theory

M. Engelhardt and B. Sperisen

*Physics Department, New Mexico State University  
Las Cruces, NM 88003, USA*

## Abstract

The question whether the center vortex picture of the strongly interacting vacuum can encompass the infrared dynamics of both  $SU(2)$  as well as  $Sp(2)$  Yang-Mills theory is addressed. These two theories contain the same center vortex degrees of freedom, and yet exhibit deconfinement phase transitions of different order. This is argued to be caused by the effective action governing the vortices being different in the two cases. To buttress this argument, a random vortex world-surface model is constructed which reproduces available lattice data characterizing  $Sp(2)$  Yang-Mills confinement properties. A new effective action term which can be interpreted in terms of a vortex stickiness serves to realize a first-order deconfinement phase transition, as found in  $Sp(2)$  Yang-Mills theory. Predictions are given for the behavior of the spatial string tension at finite temperatures.

PACS: 12.38.Aw, 12.38.Mh, 12.40.-y

Keywords: Center vortices, infrared effective theory, confinement

# 1 Introduction

The random vortex world-surface model describes the infrared, nonperturbative regime of the strong interaction on the basis of effective gluonic center vortex degrees of freedom. Such a description was initially suggested and studied in [1–5] in particular with a view towards explaining the confinement phenomenon; more recently, investigations of the relevance of center vortices in the lattice Yang-Mills ensemble [6–11], for a review, cf. [12], have provided a firm foundation for this picture. Motivated by these results, random vortex world-surface models have been formulated and studied both with respect to  $SU(2)$  as well as  $SU(3)$  Yang-Mills theory [13–18], successfully reproducing the main features of the strongly interacting vacuum. In the  $SU(2)$  case, not only has a confining low-temperature phase been obtained together with a second-order deconfinement phase transition as temperature is raised [13]; also the topological susceptibility [14, 19–22] and the (quenched) chiral condensate [15] of  $SU(2)$  Yang-Mills theory are reproduced quantitatively. In the  $SU(3)$  case, the deconfinement transition becomes weakly first order [16] and a Y-law for the baryonic static potential results in the confining phase [17].

Rather than immediately pursuing the next logical step in this development, namely, extending the  $SU(3)$  investigation to the topological and chiral properties, recent efforts have focused on the question of how far the simple random vortex world-surface concept carries if one generalizes to other gauge groups. The most obvious extension, to the  $SU(4)$  group, was reported in [23]. This study indeed confirmed the expectation formulated in [24]: As the number of colors  $N$  is increased, Abelian magnetic monopoles, which are an intrinsic feature of generic center vortices, begin to influence the distribution of vortex configurations instead of being completely enslaved to the dynamics of the vortices which host them. Unequivocal signatures of this emerge in constructing the  $SU(4)$  random vortex world-surface ensemble. Physically, the reason for this behavior is rooted in the fact that the flux emanating from Abelian magnetic monopoles is quantized in identical units for any  $N$ , whereas the flux carried by center vortices is quantized in ever smaller units as  $N$  rises. The vortices thus become “lighter” degrees of freedom in relation to the monopoles; the latter then attain a dynamical significance of their own<sup>1</sup>.

On the other hand, another systematic way of extending the Yang-Mills gauge group has recently also garnered attention [25–27]: The  $SU(2)$  group can alternatively be viewed as the smallest symplectic group  $Sp(1)$ , and the sequence of  $Sp(N)$  groups can also be used as a systematic generalization of  $SU(2) = Sp(1)$ . An interesting aspect of this sequence is that all  $Sp(N)$  have the same center,  $Z(2)$ ; furthermore, all gauge groups  $Sp(N)$  have the same first homotopy group after factoring out the center,  $\Pi_1(Sp(N)/Z(2)) = Z(2)$ . This means that they allow for the same set of center vortex degrees of freedom. The studies [25, 26] report lattice investigations of selected

---

<sup>1</sup>It should be emphasized that this does not imply that vortices cease to represent the relevant infrared degrees of freedom as the number of colors rises; all that happens is that their dynamics become more complex, and cannot be described purely in terms of world-surface characteristics anymore.

$Sp(N)$  Yang-Mills theories; the data gathered there now provide an opportunity to confront the random vortex world-surface model with these theories. In particular, while  $SU(2) = Sp(1)$  Yang-Mills theory exhibits a second-order deconfinement phase transition, the transition is first order in  $Sp(2)$  Yang-Mills theory. Thus, one has two Yang-Mills theories with the same center and center vortex content which display completely different behavior at the deconfinement transition. This raises the question whether center vortices indeed are the relevant degrees of freedom determining the physics of confinement and, in particular, the transition to a deconfined high-temperature phase. Of course, whereas the infrared effective vortex models corresponding to  $SU(2)$  and  $Sp(2)$  Yang-Mills theory are based on the same set of vortex degrees of freedom, the respective effective vortex actions may be quite different; after all, they formally result from integrating out the very different cosets of the two gauge groups. Thus, a different behavior of the two models at the deconfinement transition is by no means excluded. Nevertheless, it would be useful to buttress this argument by an explicit construction of a random vortex world-surface model for  $Sp(2)$  Yang-Mills theory, to demonstrate that the vortex picture can encompass the confinement physics of both the  $SU(2)$  and the  $Sp(2)$  cases. To furnish such a construction is the objective of the present work.

## 2 $Sp(2)$ lattice Yang-Mills theory data

The objective of the present investigation is to find a  $Z(2)$ -symmetric random vortex world-surface model with a first-order deconfinement phase transition and, if possible, adjust it to reproduce known data on  $Sp(2)$  Yang-Mills theory. Two relevant quantitative characteristics are reported in [25], namely, the ratio of the deconfinement temperature to the square root of the zero-temperature string tension,  $T_c/\sqrt{\sigma}$ , and the latent heat  $L_H$ . The latent heat corresponds to the discontinuity in the four-dimensional action density<sup>2</sup>  $\bar{s}$  at the first-order deconfinement transition, and is given in [25] in units of the lattice spacing  $a$ , i.e.,  $L_H = a^4\Delta\bar{s}$ . While [25] gives  $T_c/\sqrt{\sigma}$  for a number of  $Sp(2)$  lattice Yang-Mills couplings and the extrapolation to the continuum limit,  $L_H$  is only reported quantitatively for one coupling,  $8/g^2 = 6.4643$ ; it should be noted that the scaling regime does not quite extend to that strong a coupling. In view of these data, it seems most consistent to model  $Sp(2)$  Yang-Mills theory specifically at the aforementioned coupling,  $8/g^2 = 6.4643$ , as opposed to using a mixed input data set consisting of the continuum limit of  $T_c/\sqrt{\sigma}$  on the one hand and the value of  $L_H$  at  $8/g^2 = 6.4643$  on the other hand.

At  $8/g^2 = 6.4643$ , one has [25]

$$T_c/\sqrt{\sigma} = 0.59 \tag{1}$$

---

<sup>2</sup>Since the symbol  $s$  will serve a different purpose below, the action density is denoted  $\bar{s}$  here and in the following.

(in the continuum limit, this value rises to 0.69). On the other hand, identifying  $L_H = a^4 \Delta \bar{s}$ , the action density discontinuity  $\Delta \bar{s}$  satisfies [25]

$$N_t(a^4 \Delta \bar{s})^2/4 = 0.15 \quad (2)$$

where  $N_t$  denotes the extent of the lattice in the (Euclidean) time direction. Taking into account that, at this coupling, the deconfinement transition occurs at  $N_t = 2$ , i.e., the deconfinement temperature is given by  $T_c a = 1/2$ , one can eliminate the lattice spacing, yielding

$$\Delta \bar{s}/T_c^4 = 8.76 \quad (3)$$

The two relations (1) and (3) will serve as input data for the random vortex world-surface model constructed below.

### 3 Random vortex world-surface model

Center vortices are closed tubes of quantized chromomagnetic flux in three spatial dimensions. In four-dimensional (Euclidean) space-time, they are therefore represented by (thickened) world-surfaces. The quantization of flux is defined by the center of the gauge group; a Wilson loop linked to a vortex yields a nontrivial center element (the trivial unit element signals absence of any flux). For gauge groups with a  $Z(2)$  center, such as the  $SU(2)$  case studied in [13–15] or the  $Sp(2)$  case studied here, this implies that there is only one type of vortex flux, corresponding to the only nontrivial center element  $(-1)$ .

The model construction used in the following is entirely analogous to the  $SU(2)$  model [13], and the reader is referred to that work for further details regarding the construction and interpretation of random vortex world-surface models. As argued in the introductory section further above, differences between the  $SU(2)$  and  $Sp(2)$  models arise only at the level of the effective vortex action, discussed further below. Apart from that discussion, thus, a brief overview of the modeling methodology shall suffice:

In order to arrive at a tractable model description, vortex world-surfaces are composed of elementary squares on a hypercubic lattice. The lattice square extending from the site  $x$  into the positive  $\mu$  and  $\nu$  directions (where, for definiteness,  $\mu < \nu$ ) is associated with a value  $q_{\mu\nu}(x) \in \{0, 1\}$ , where the value 1 means that the square is part of a vortex surface and the value 0 means it is not<sup>3</sup>. For ease of notation below, it is useful to define also  $q_{\nu\mu}(x) = q_{\mu\nu}(x)$ . An ensemble of vortex world-surface configurations is generated by Monte Carlo update. In order to preserve the closed character of the world-surfaces, an elementary update acts on all six squares forming the surface of an elementary three-dimensional cube in the four-dimensional lattice. If the cube extends

---

<sup>3</sup>Note that this is adequate for the description of confinement properties, since the Wilson loop is insensitive to flux orientation. To treat topological and chiral properties, a slightly extended description, which permits the specification of vortex orientation, is needed [14, 15].

from the site  $x$  into the positive  $\mu$ ,  $\nu$  and  $\lambda$  directions, then an update simultaneously effects

$$\begin{aligned} q_{\mu\nu}(x) &\rightarrow 1 - q_{\mu\nu}(x), & q_{\mu\nu}(x + e_\lambda) &\rightarrow 1 - q_{\mu\nu}(x + e_\lambda), \\ q_{\nu\lambda}(x) &\rightarrow 1 - q_{\nu\lambda}(x), & q_{\nu\lambda}(x + e_\mu) &\rightarrow 1 - q_{\nu\lambda}(x + e_\mu), \\ q_{\lambda\mu}(x) &\rightarrow 1 - q_{\lambda\mu}(x), & q_{\lambda\mu}(x + e_\nu) &\rightarrow 1 - q_{\lambda\mu}(x + e_\nu). \end{aligned} \quad (4)$$

In practice, sweeps through the lattice are performed in which updates involving all three-dimensional cubes in the lattice are considered in turn.

One important point which should be noted is the interpretation of the lattice spacing [13]. In random vortex world-surface models, the lattice spacing is a fixed physical quantity, which in the  $SU(2)$  and  $SU(3)$  cases is determined [13, 16] to be 0.39 fm (where the scale is set by defining the zero-temperature string tension  $\sigma$  to be  $\sigma = (440 \text{ MeV})^2$ ). Physically, this introduces into the models the notion that vortices possess a certain transverse thickness. While they are formally represented as two-dimensional surfaces, the fixed lattice spacing prevents, e.g., two parallel vortices from propagating at such a short distance from one another that they would cease to be mutually distinguishable if their transverse profile were explicitly taken into account. Random vortex world-surface models are thus infrared effective theories with a fixed ultraviolet cutoff in form of a fixed lattice spacing determined by the physical vortex thickness.

As mentioned above, the substantive difference between the  $SU(2)$  vortex model studied in [13–15] and the  $Sp(2)$  vortex model arises at the level of the vortex effective action used in the Monte Carlo generation of the vortex ensemble. In the  $SU(2)$  (and also the  $SU(3)$ ) model, one action term (and, therefore, one adjustable dimensionless parameter) is sufficient to achieve quantitative agreement between infrared observables studied in the vortex model and the data from the corresponding full lattice Yang-Mills theory. The action term in question is a world-surface curvature term,

$$\begin{aligned} S_c[q] &= c \sum_x \sum_\mu \left[ \sum_{\substack{\nu < \lambda \\ \nu \neq \mu, \lambda \neq \mu}} (q_{\mu\nu}(x) q_{\mu\lambda}(x) + q_{\mu\nu}(x) q_{\mu\lambda}(x - e_\lambda) \right. \\ &\quad \left. + q_{\mu\nu}(x - e_\nu) q_{\mu\lambda}(x) + q_{\mu\nu}(x - e_\nu) q_{\mu\lambda}(x - e_\lambda)) \right] \\ &= \frac{c}{2} \sum_x \sum_\mu \left[ \left[ \sum_{\nu \neq \mu} (q_{\mu\nu}(x) + q_{\mu\nu}(x - e_\nu)) \right]^2 - \sum_{\nu \neq \mu} [q_{\mu\nu}(x) + q_{\mu\nu}(x - e_\nu)]^2 \right]. \end{aligned} \quad (5)$$

As can be read off from the first expression, for each link in the lattice, all pairs of elementary squares attached to that link, but not lying in one plane, are examined. If both members of such a pair are part of a lattice surface, this costs an action increment  $c$ . Thus, vortex surfaces are penalized for “turning a corner”, i.e., for their curvature.

It should be noted that also an action term of the Nambu-Goto type, proportional to the world-surface area, was considered for the  $SU(2)$  and  $SU(3)$  models [13, 16]. The

result of these considerations is that, in practice, the effect of such a term can be absorbed into the curvature term. Including it does not enhance the phenomenological flexibility of the models appreciably, and it was therefore ultimately dropped. In particular, no indication has been found that a world-surface area term would be useful for the purpose of driving the deconfinement phase transition towards first-order behavior, as is necessary for an accurate modeling of  $Sp(2)$  Yang-Mills theory.

The desired first-order behavior therefore has to be generated by different dynamics. A promising strategy in this regard is suggested by the experience gathered with the  $SU(4)$  random vortex world-surface model [23]. Also in that case, it was necessary to devise dynamics which enhance the first-order character of the deconfinement transition. A viable solution was found to be an action term which enhances vortex branching.  $SU(4)$  Yang-Mills theory allows for two physically distinct types of center vortices, and the associated chromomagnetic flux can combine and disassociate, thus creating a branched structure of the world-surface configurations. In the present case, there is only one type of vortex flux, and branching is consequently impossible. However, an effect reminiscent of branching behavior can be envisaged: In terms of world-surfaces composed of elementary squares on a lattice, branching essentially means that more than two squares attached to a given link are part of a vortex. This notion can indeed be translated to the case studied here, albeit with a different physical interpretation. In the present vortex model, it is possible for two (or even three) vortex surfaces to share a lattice link; in this case, four (or even six) elementary squares attached to the link are part of a vortex. In terms of the propagation of vortex lines in three dimensions, this corresponds to two (or even three) lines meeting at a point in three-dimensional space and remaining attached to one another for a finite length in the fourth direction before separating again. Enhancing such behavior can be interpreted as making the vortices more “sticky”. Therefore, a promising avenue is the introduction of a vortex stickiness term into the action,

$$S_s[q] = \sum_x \sum_\mu F \left( \sum_{\nu \neq \mu} (q_{\mu\nu}(x) + q_{\mu\nu}(x - e_\nu)) \right) \quad (6)$$

where

$$F(4) = s_4, \quad F(6) = s_6, \quad F = 0 \text{ else.} \quad (7)$$

Thus, for each link in the lattice, if four elementary squares attached to the link are part of a vortex, this is weighted by an action increment  $s_4$ ; if six elementary squares attached to the link are part of a vortex, this is weighted by an action increment  $s_6$ . Choosing negative values of  $s_4$  and  $s_6$  facilitates such behavior, corresponding to the vortices becoming more sticky. In general,  $s_4$  and  $s_6$  are independent parameters. However, for the remainder of the present investigation, only the case  $s_4 \equiv s_6 \equiv s$  is considered further, with the complete action

$$S[q] = S_c[q] + S_s[q] \quad (8)$$

depending on two dimensionless parameters  $c$  and  $s$ . In the absence of the term  $S_s[q]$ , the deconfinement phase transition is second order, and a viable model for the infrared sector of  $SU(2)$  Yang-Mills theory is achieved [13] for  $c = 0.24$ . As will be seen below, introducing  $S_s[q]$  indeed serves to induce first-order behavior at the deconfinement transition for sufficiently negative  $s$ , and the characteristics of  $Sp(2)$  lattice Yang-Mills theory listed in section 2 can be reproduced.

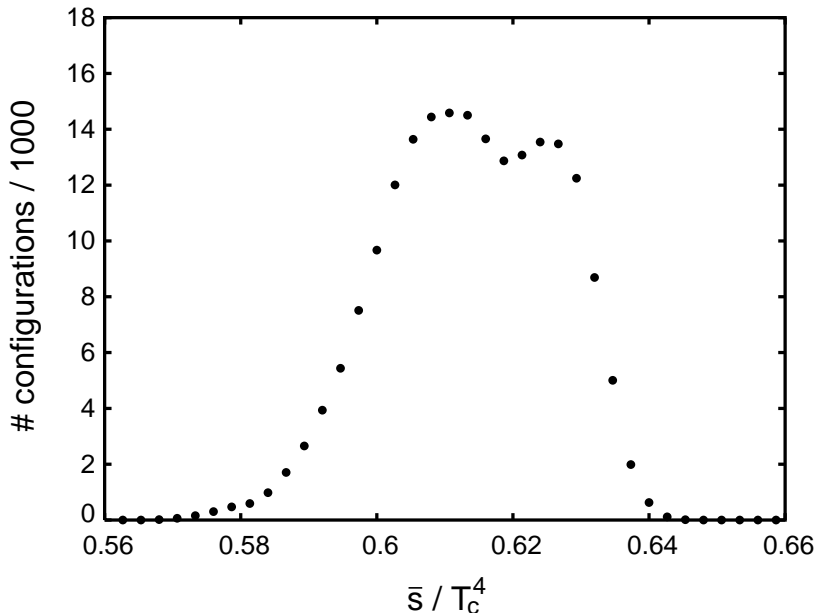


Figure 1: Distribution of the four-dimensional action density  $\bar{s}$  at the deconfinement phase transition, for coupling parameters  $c = 0.3394$  and  $s = -1.24$ . The measurement was taken on a  $50^3 \times 1$  lattice.

## 4 Locating the physical point

On the basis of the above model definition, Monte Carlo measurements of observables can be carried out. The observables relevant for the comparison with the  $Sp(2)$  lattice Yang-Mills data given in section 2 are, on the one hand, the probability distribution of the action density and, on the other hand, Wilson loops, from which string tensions can be extracted. The value of a Wilson loop in any given vortex configuration is determined by the defining property of vortex flux: Each instance of a vortex surface piercing an area spanned by the loop<sup>4</sup> contributes a phase factor  $(-1)$  to the value of the

<sup>4</sup>Wilson loops are defined on a lattice which is dual to the one on which the vortices are constructed; thus, vortex piercings of areas spanned by Wilson loops are defined unambiguously.

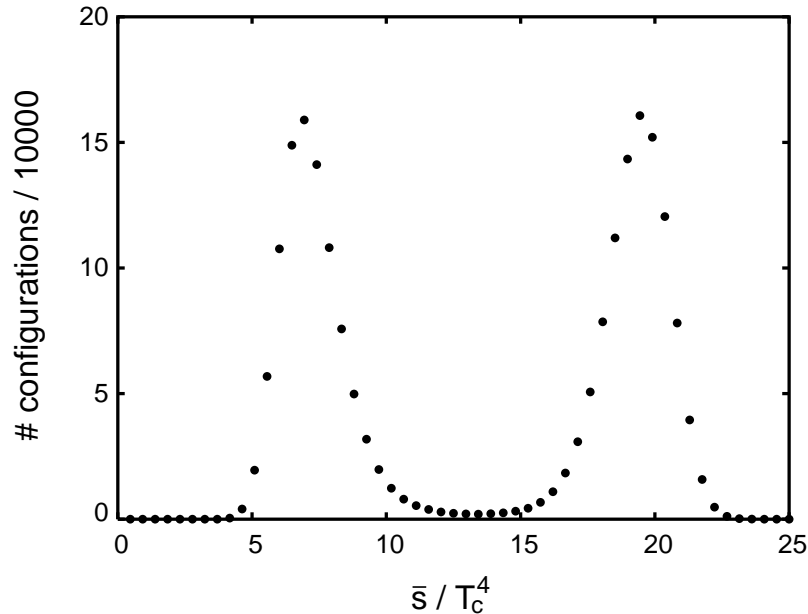


Figure 2: Distribution of the four-dimensional action density  $\bar{s}$  at the deconfinement phase transition, for coupling parameters  $c = 0.5469$  and  $s = -1.99$ . The measurement was taken on a  $6^3 \times 2$  lattice.

Wilson loop. The action density probability distribution is used to detect a first-order deconfinement phase transition via a double-peak structure signaling the coexistence of two phases. Examples of such action density distributions are given in Figs. 1-5. The distance between the peaks in these distributions gives a measure for the action density discontinuity  $\Delta\bar{s}$  at the transition. The corresponding values extracted from Figs. 1-5 are reported in Tables 1 and 2 further below.

Since the lattice spacing in random vortex world-surface models is a fixed physical quantity, only a discrete set of temperatures can be accessed for a given set of coupling parameters  $c$  and  $s$ . Therefore, in general one cannot expect to realize the deconfinement transition directly at the physical values of  $c$  and  $s$  which correctly model full  $Sp(2)$  lattice Yang-Mills theory; the inverse deconfinement temperature usually will not be an integer multiple of the lattice spacing at the physical point. For this reason, one has to resort to an interpolation procedure [13]: The deconfinement transition is studied at unphysical values of  $c$  and  $s$ , on lattices extending a varying number  $N_t$  of spacings in the (Euclidean) time direction, and the properties of the transition at the physical point are obtained by interpolation. In the following, two such schemes will be investigated, one based on lattices with  $N_t = 1, 2$  and one based on lattices with  $N_t = 1, 2, 3$ . By trial and error, one can find sets of coupling parameters  $c$  and  $s$  which yield a double peak in the action density distribution, i.e., which realize the deconfinement transition, cf. Figs. 1-

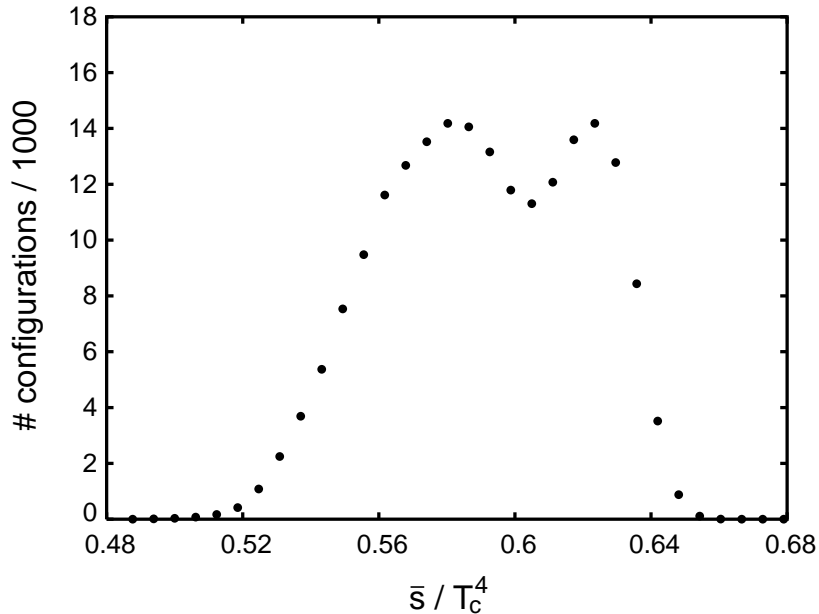


Figure 3: Distribution of the four-dimensional action density  $\bar{s}$  at the deconfinement phase transition, for coupling parameters  $c = 0.3513$  and  $s = -1.3$ . The measurement was taken on a  $30^3 \times 1$  lattice.

5. For these parameter sets, one therefore knows the deconfinement temperature  $T_c$  in lattice units,  $aT_c = 1/N_t$ , and one can read off the action density discontinuity in lattice units  $a^4 \Delta \bar{s}$ , in which  $a$  can be eliminated in favor of  $T_c$ . Measuring in addition the zero-temperature string tension in lattice units,  $\sigma a^2$ , one can furthermore determine the ratio  $T_c / \sqrt{\sigma}$ . Such data sets are given below in Tables 1 and 2.

Before discussing these data sets, it should be noted that the requirement of finding the deconfinement phase transition on a given lattice fixes only one of the two coupling parameters  $c$  and  $s$ . For a wide range of  $c$ , one can find an appropriate  $s$  realizing the transition, and vice versa. The pairs of  $c$  and  $s$  for which data are reported below were singled out, through extensive trial and error, by the additional requirement that interpolation of these data sets must indeed yield the physical point, i.e., must simultaneously yield the correct  $Sp(2)$  values for  $T_c / \sqrt{\sigma}$  and  $\Delta \bar{s} / T_c^4$  given in section 2. Choosing a suitable point on an interpolation trajectory always allows one to fit one of those values, but there is no guarantee that the other one will simultaneously be correct. This is a nontrivial additional constraint requiring a substantial search in the space of coupling parameters  $c$  and  $s$ . The final result of that search is the specific set of data reported in Tables 1 and 2.

Table 1 displays suitable data sets found on lattices with  $N_t = 1, 2$ . Since two data points are available for each quantity, all quantities can be interpolated as linear func-

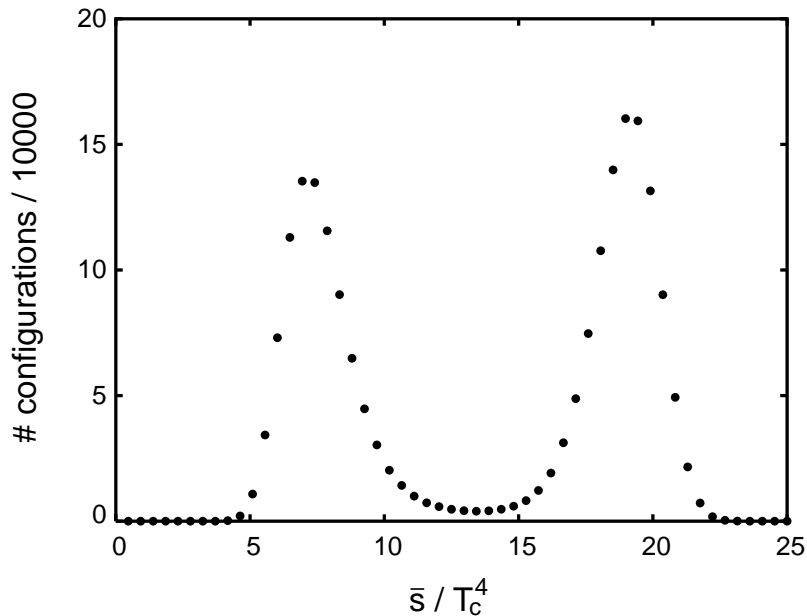


Figure 4: Distribution of the four-dimensional action density  $\bar{s}$  at the deconfinement phase transition, for coupling parameters  $c = 0.5337$  and  $s = -1.9$ . The measurement was taken on a  $6^3 \times 2$  lattice.

tions of one parameter. Choosing that parameter to be one of the relevant observables,  $T_c/\sqrt{\sigma}$ , one immediately verifies that  $\Delta\bar{s}/T_c^4 = 8.76$  is indeed realized for  $T_c/\sqrt{\sigma} \approx 0.59$ , as required by (1) and (3). Similarly, for that value of  $T_c/\sqrt{\sigma}$ , the coupling parameters  $c$  and  $s$  interpolate to

$$c = 0.479, \quad s = -1.745, \quad (9)$$

defining their physical values. Finally,  $aT_c$  as a linear function of  $T_c/\sqrt{\sigma}$  interpolates to

$$aT_c = 0.663, \quad (10)$$

implying that the inverse deconfinement temperature lies between  $a$  and  $2a$ , but is near

| $c$    | $s$   | $aT_c$ | $\Delta\bar{s}/T_c^4$ | $T_c/\sqrt{\sigma}$ |
|--------|-------|--------|-----------------------|---------------------|
| 0.3394 | -1.24 | 1      | 0.014                 | 0.816               |
| 0.5469 | -1.99 | 0.5    | 13                    | 0.474               |

Table 1: Sets of coupling parameters  $c$ ,  $s$  realizing the deconfinement phase transition on lattices with  $N_t = 1, 2$ , together with values for the action density discontinuity extracted from Figs. 1 and 2 and measurements of the ratio of the deconfinement temperature to the square root of the zero-temperature string tension.

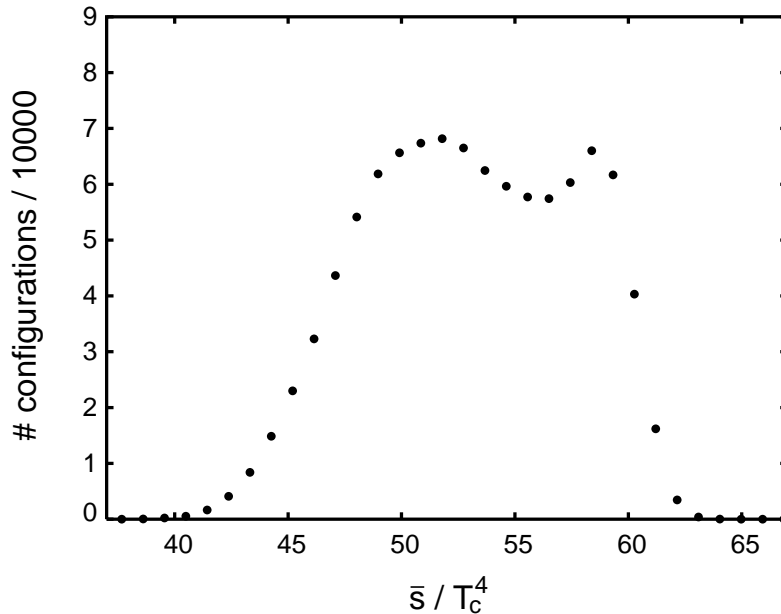


Figure 5: Distribution of the four-dimensional action density  $\bar{s}$  at the deconfinement phase transition, for coupling parameters  $c = 0.4546$  and  $s = -0.3$ . The measurement was taken on a  $16^3 \times 3$  lattice.

neither of those two values; the physical point is not close to either of the two data sets listed in Table 1. This is different from the  $SU(N)$  models investigated in [13, 16, 23]; in those cases, the physical point is very near the  $N_t = 2$  data set and the interpolation procedure only introduces small corrections to that set in defining the physical point. In the present  $Sp(2)$  case, the uncertainty inherent in the interpolation procedure is much more substantial due to the distance of the physical point from any of the data sets reported in Table 1.

One straightforward consistency check of the interpolation can be made as follows. Up to this point, all quantities at the physical point have been defined by interpolation of the data in Table 1. In the case of the deconfinement transition characteristics, one has no choice in the matter, since these are not directly accessible at the physical point (9). However, the zero-temperature string tension can be measured independently directly at the physical point. The result of such a measurement, combined with (10), again yields the correct value  $T_c/\sqrt{\sigma} = 0.59$ , buttressing the validity of the interpolation procedure.

On the other hand, another way to gain insight into the uncertainty of the interpolation lies in using an expanded data set obtained on lattices with  $N_t = 1, 2, 3$  and comparing with the results obtained above. Table 2 displays corresponding suitable data. Since three data points are available for each quantity, all quantities can be interpolated as parabolas depending on one parameter. Here, a difficulty arises which is not

| $N_t$ | $c$    | $s$  | $\Delta\bar{s}/T_c^4$ | $T_c/\sqrt{\sigma}$ |
|-------|--------|------|-----------------------|---------------------|
| 1     | 0.3513 | -1.3 | 0.040                 | 0.810               |
| 2     | 0.5337 | -1.9 | 12                    | 0.485               |
| 3     | 0.4546 | -0.3 | 7.3                   | 0.480               |

Table 2: Sets of coupling parameters  $c$ ,  $s$  realizing the deconfinement phase transition on lattices with  $N_t = 1, 2, 3$ , together with values for the action density discontinuity extracted from Figs. 3-5 and measurements of the ratio of the deconfinement temperature to the square root of the zero-temperature string tension.

present in the linear interpolation scheme discussed further above: One cannot simply choose either of the two physical dimensionless ratios  $T_c/\sqrt{\sigma}$  or  $\Delta\bar{s}/T_c^4$  as the interpolation parameter, because the former is very closely spaced between the  $N_t = 2$  and the  $N_t = 3$  data sets, leading to an extremely unstable interpolation, and the latter is not even monotonous as  $N_t$  rises. Consequently, to have well-spaced interpolation points conducive to a stable interpolation, in the present case,  $N_t$  was used as the interpolation parameter. The drawback is, of course, that the entire procedure becomes more indirect; both of the quantities of primary interest,  $T_c/\sqrt{\sigma}$  and  $\Delta\bar{s}/T_c^4$ , are interpolated as a function of a third parameter, instead of one being interpolated directly as a function of the other. Constructing the corresponding parabolas in  $N_t$ , one indeed verifies that the relations (1) and (3) for  $T_c/\sqrt{\sigma}$  and  $\Delta\bar{s}/T_c^4$  are simultaneously satisfied for  $N_t = 1.5573$ . Furthermore, at that value of  $N_t$ , the parabolas for the coupling parameters  $c$  and  $s$  yield

$$c = 0.485 , \quad s = -1.90 , \quad (11)$$

defining the physical point in this interpolation scheme. Finally, identifying  $aT_c = 1/N_t$ , one has at the physical point

$$aT_c = 0.642 . \quad (12)$$

Also this interpolation scheme can be cross-checked by independently calculating the zero-temperature string tension in lattice units,  $\sigma a^2$ , at the point (11) in the space of coupling parameters, and combining this with (12) to obtain another determination of  $T_c/\sqrt{\sigma}$ . This yields the value  $T_c/\sqrt{\sigma} = 0.52$ , deviating significantly from the interpolated value  $T_c/\sqrt{\sigma} = 0.59$ . Despite extensive search in the space of coupling constants, the authors were unable to find a more consistent data set. Thus, the interpolation scheme using  $N_t = 1, 2, 3$  appears to be less reliable<sup>5</sup> than the one using  $N_t = 1, 2$ . In view

---

<sup>5</sup>In general, there is no guarantee that the interpolating polynomial becomes more accurate as more values of  $N_t$  are added to the data set, especially values which are distant from the physical point; interpolation can become less stable as its order is increased. Also from a more physical point of view, at  $N_t = 3$ , the vortex model constructed here is already rather far removed from the infrared  $Sp(2)$  physics of interest, and including data from this case may well have the effect of distorting the physical picture rather than improving convergence.

of this, the set of coupling constants (9) will be regarded in the following as the best approximation to the physical point, and deviations obtained using the set (11) will be taken as an indication of the systematic uncertainty inherent in the interpolation procedure. Comparing (9) with (11), as well as (10) with (12), these uncertainties appear to be under 10%. A further such comparison will be possible for the spatial string tensions discussed below, similarly leading to an error estimate of around 10%.

## 5 Predictions for the spatial string tension

On the basis of the model for the infrared sector of  $Sp(2)$  Yang-Mills theory constructed above, predictions of further physical quantities can be made. One important nonperturbative characteristic of Yang-Mills theory is the behavior of the spatial string tension  $\sigma_S$  at finite temperatures. Using the physical set of coupling parameters (9), measurements on lattices with  $N_t = 1, 2, 3$  yield the results listed in Table 3, where  $N_t$  has been translated into  $T/T_c$  using (10).

|                             |      |      |      |
|-----------------------------|------|------|------|
| $T/T_c$                     | 0.50 | 0.75 | 1.51 |
| $\sigma_S(T)/\sigma_S(T=0)$ | 1.00 | 1.02 | 1.36 |

Table 3: Predictions for the behavior of the spatial string tension  $\sigma_S$  at finite temperatures, normalized to the zero-temperature value  $\sigma_S(T=0) \equiv \sigma$ .

The characteristic rise of the spatial string tension in the deconfined phase observed in  $SU(N)$  Yang-Mills theories is predicted to occur also in the  $Sp(2)$  case, Table 3 giving a quantitative measure for this behavior. By carrying out corresponding measurements within  $Sp(2)$  lattice Yang-Mills theory, the validity of the vortex model constructed here can be put to test. To obtain an indication of the systematic uncertainty in the above predictions, engendered by the interpolation procedure used in defining the physical point, it is useful to calculate the spatial string tension also for the alternate set of coupling parameters (11). This yields the results displayed in Table 4.

|                             |      |      |      |
|-----------------------------|------|------|------|
| $T/T_c$                     | 0.52 | 0.78 | 1.56 |
| $\sigma_S(T)/\sigma_S(T=0)$ | 1.00 | 1.01 | 1.2  |

Table 4: Behavior of the spatial string tension  $\sigma_S$  at finite temperatures, normalized to the measured zero-temperature value  $\sigma_S(T=0) \equiv \sigma$ , for the alternate set of coupling parameters (11). Deviations compared to Table 3 give an indication of the systematic uncertainty in predicting the spatial string tension.

When using the coupling parameters (11), the discussion following eq. (12) should be kept in mind: Already the measurement of the zero-temperature string tension us-

ing (11) leads, combined with (12), to a significant deviation from the correct value  $T_c/\sqrt{\sigma} = 0.59$ . Thus, the spatial string tension measurement at finite temperatures can be expected to suffer from similar distortions. Table 4 therefore gives the ratio of the finite-temperature spatial string tension measured using (11) to the zero-temperature string tension *measured* using (11). This should cancel the distortions to some extent; in particular, it leads to the correct low-temperature limit. For the highest temperature displayed, Table 4 displays a ratio which is roughly 10% below the value in Table 3. In comparison, if one used a value for the zero-temperature string tension consistent with  $T_c/\sqrt{\sigma} = 0.59$ , then that ratio would rise to a value roughly 10% above the value in Table 3. Altogether, therefore, the systematic uncertainty also in the case of the predictions given in Table 3 is of the order of 10%, similar to the quantities considered in section 4.

## 6 Conclusions

The main objective of the present work was to demonstrate, by explicit construction of a corresponding random vortex world-surface model, that the center vortex picture can encompass the infrared physics of both  $SU(2)$  and  $Sp(2)$  Yang-Mills theory. Doubts in this respect had recently arisen in some quarters, based on the observation that the two Yang-Mills theories contain the same center vortex degrees of freedom, and yet exhibit qualitatively different behavior at the deconfinement phase transition, as demonstrated in [25–27]. To resolve this apparent dichotomy, it is necessary to take into account that, while  $SU(2)$  and  $Sp(2)$  Yang-Mills theory contain the same center vortex degrees of freedom, the effective actions governing those degrees of freedom are different; after all, different cosets would have to be integrated out if one were to derive those effective actions from the underlying Yang-Mills theories. Thus, there is no obstacle in principle to both theories being described by vortex models in the infrared sector; the present investigation set out to show that such descriptions can indeed be achieved in practice.

Within the random vortex world-surface model, the vortex effective action is determined phenomenologically. As shown in the present work, the introduction of a vortex “stickiness” provides a way to drive the deconfinement phase transition towards first-order behavior, which is necessary for a correct description of the transition in the  $Sp(2)$  case. By adjusting the stickiness and curvature coefficients in the vortex effective action, agreement with known data from  $Sp(2)$  lattice Yang-Mills theory was achieved, subject to systematic uncertainties engendered by the interpolation procedure which is necessary to define the deconfinement transition properties at the physical point. While these uncertainties remained small in the  $SU(N)$  random vortex world-surface models studied previously [13–18, 23], in the  $Sp(2)$  case, they are sizeable, and are estimated to amount to roughly 10 % for the observables studied here. Subject to this caveat, the results of the present modeling effort indeed support the notion that  $Sp(2)$  Yang-Mills theory can be described in terms of vortex dynamics in the infrared, along with the

$SU(2)$  case investigated in [13–15]. The predictions for the spatial string tension at finite temperatures presented in Table 3 above provide a further opportunity to test this notion, through comparison with corresponding measurements within  $Sp(2)$  lattice Yang-Mills theory.

## Acknowledgments

This work was supported by the U.S. DOE under grants DE-FG03-95ER40965 (M.E.) and DE-FG02-94ER40847 (B.S.).

## References

- [1] G. 't Hooft, Nucl. Phys. **B138** (1978) 1.
- [2] Y. Aharonov, A. Casher and S. Yankielowicz, Nucl. Phys. **B146** (1978) 256.
- [3] J. M. Cornwall, Nucl. Phys. **B157** (1979) 392.
- [4] G. Mack, Phys. Rev. Lett. **45** (1980) 1378.
- [5] H. B. Nielsen and P. Olesen, Nucl. Phys. **B160** (1979) 380.
- [6] L. Del Debbio, M. Faber, J. Greensite and Š. Olejník, Phys. Rev. D **55** (1997) 2298.
- [7] L. Del Debbio, M. Faber, J. Giedt, J. Greensite and Š. Olejník, Phys. Rev. D **58** (1998) 094501.
- [8] T. G. Kovács and E. T. Tomboulis, Phys. Rev. D **57** (1998) 4054.
- [9] P. de Forcrand and M. D'Elia, Phys. Rev. Lett. **82** (1999) 4582.
- [10] M. Engelhardt, K. Langfeld, H. Reinhardt and O. Tennert, Phys. Lett. **B431** (1998) 141.
- [11] M. Engelhardt, K. Langfeld, H. Reinhardt and O. Tennert, Phys. Rev. D **61** (2000) 054504.
- [12] J. Greensite, Prog. Part. Nucl. Phys. **51** (2003) 1.
- [13] M. Engelhardt and H. Reinhardt, Nucl. Phys. **B585** (2000) 591.
- [14] M. Engelhardt, Nucl. Phys. **B585** (2000) 614.
- [15] M. Engelhardt, Nucl. Phys. **B638** (2002) 81.
- [16] M. Engelhardt, M. Quandt and H. Reinhardt, Nucl. Phys. **B685** (2004) 227.
- [17] M. Engelhardt, Phys. Rev. D **70** (2004) 074004.
- [18] M. Quandt, H. Reinhardt and M. Engelhardt, Phys. Rev. D **71** (2005) 054026.
- [19] J. M. Cornwall, Phys. Rev. D **61** (2000) 085012.

- [20] M. Engelhardt and H. Reinhardt, Nucl. Phys. **B567** (2000) 249.
- [21] R. Bertle, M. Engelhardt and M. Faber, Phys. Rev. D **64** (2001) 074504.
- [22] F. Bruckmann and M. Engelhardt, Phys. Rev. D **68** (2003) 105011.
- [23] M. Engelhardt, Phys. Rev. D **73**, 034015 (2006).
- [24] J. Greensite and Š. Olejník, JHEP **0209** (2002) 039.
- [25] K. Holland, M. Pepe, and U.-J. Wiese, Nucl. Phys. **B694** (2004) 35.
- [26] M. Pepe, Nucl. Phys. Proc. Suppl. **141** (2005) 238.
- [27] M. Pepe, PoS **LAT2005** (2005) 017.